J Mol Model (2013) 19:1301–1309
DOI 10.1007/s00894-012-1680-0

ORIGINAL PAPER

Constant pH molecular dynamics (CpHMD) and molecular docking studies of CquiOBP1 pH-induced ligand releasing mechanism

Wen-Ting Chu · Ji-Long Zhang · Qing-Chuan Zheng · Lin Chen · Yun-Jian Wu · Qiao Xue · Hong-Xing Zhang

Received: 11 May 2012 / Accepted: 5 November 2012 / Published online: 24 November 2012

Abstract The odorant binding protein of *Culex quinquefasciatus* (CquiOBP1), expressed on the insect antenna, is crucial for the investigation of trapping baited with oviposition semi-chemicals and controlling mosquito populations. The acidic titratable residues pKa prediction and the ligand binding poses investigation in two systems (pH 7 and pH 5) are studied by constant pH molecular dynamics (CpHMD) and molecular docking methods. Research results reveal that the change of the protonation states would disrupt some important H-bonds, such as Asp 66-Asp 70, Glu 105-Asn 102, etc. The cleavage of these H-bonds leads to the movement of the relative position of hydrophobic tunnel, N- and C- termini loops and pH-sensing triad (His23-Tyr54-Val125) in acid solution. Ligand MOP has lower affinity and shows different binding poses to protein CquiOBP1 at pH 5. This ligand may be released from another tunnel between helices α3 and α4 in acidic environment. However, it would bind to the protein with high affinity in neutral environment. This work could provide more penetrating understanding of the pH-induced ligand-releasing mechanism.

Keywords Docking · Odorant binding protein · pKa prediction

Electronic supplementary material The online version of this article (doi:10.1007/s00894-012-1680-0) contains supplementary material, which is available to authorized users.

W.-T. Chu · J.-L. Zhang · Q.-C. Zheng (✉) · L. Chen · Y.-J. Wu · Q. Xue · H.-X. Zhang (✉)
State Key Laboratory of Theoretical and Computational Chemistry, Institute of Theoretical Chemistry, Jilin University, Changchun 130023, People's Republic of China
e-mail: zhengqc@jlu.edu.cn
e-mail: zhanghx@mail.jlu.edu.cn

Introduction

The insect odorant binding proteins (OBPs) are small soluble proteins (about 15 kDa) with high structural homology, all containing six helices (α1–α6) and three disulfide bridges [1–3]. These proteins belong to two major classes, pheromone-binding proteins (PBPs) and general odorants-binding proteins (GOBPs) [4, 5]. So far, a lot of structures of insect OBPs have been published, which can be divided into three classes by length: long-chain OBPs (about 140 amino acids), such as Lepidopteran *Bombyx mori* (BmorPBP) and *Antheraea polyphemus* (ApolPBP); middle-chain OBPs (about 120 amino acids), such as dipteran *Culex quinquefasciatus* (CquiOBP1), *Anopheles gambiae* (AgamOBP1) and *Aedes aegypti* (AaegOBP1); short-chain OBPs (about 100 amino acids).

The main function of OBPs is transporting chemical signals (semiochemicals), for example odorants and pheromones, to cross the aqueous sensillar lymph to the olfactory receptors (ORs) before reaching the neuronal membrane. Some insects, such as *Culex quinquefasciatus*, *Anopheles gambiae*, and *Aedes aegypti*, are major vectors of malaria, filariasis, and cephalitis transmission all around the world [6, 7]. Most insect OBPs have a pH-dependent feature, which makes them show high affinity with their ligands at high pH but show no or lower affinity at low pH [8]. Heretofore there have been numerous studies of the BmorPBP and ApolPBP, including experiments and theoretics investigations [9–11].

In this paper we choose the odorant binding protein of *Culex quinquefasciatus* (CquiOBP1) for research (PDB code: 3OGN). For its shorter C-terminus, CquiOBP1 has a different mechanism to the BmorPBP and ApolPBP, its C-terminus makes up part of the central cavity wall in neutral solution. Binding assays by Leal et al. in 2008 obviously

showed that its ligand mosquito oviposition pheromone (MOP, (*5R*,*6S*)-6-acetoxy-5-hexadecanolide) bound to CquiOBP1 at pH 7 with high affinity, but with very low affinity at pH 5 [8]. In 2009, Leite et al. reported that the loss of affinity had something to do with the disruption of hydrogen bond network between the conserved pH-sensing triad [12]. Later in 2010, Yang et al. hypothesized that the disruption would be caused by the displacement of C terminus from the central cavity [13]. However, there has been no detailed study for the pKa prediction and the ligand release mechanism yet. In our study, the aim is to discover the structures of CquiOBP1 at pH 5 and pH 7 with the constant pH molecular dynamics (CpHMD) method, respectively, and find out which leads to the structural changes. Furthermore, using docking studies, we can detect which structure shows higher affinity to the ligand MOP. Here we report the CpHMD and docking results of CquiOBP1, which illustrate close agreement between theoretical and experimental results, and may be helpful for further mechanism investigation.

Materials and methods

Traditionally, molecular dynamics (MD) simulations have employed constant protonation states for titratable residues, which have many drawbacks. Constant pH molecular dynamics (CpHMD) is a useful theoretical method to simulate the structure change of proteins according to acidic or basic solution. CpHMD methods can be largely classified into two categories, discrete and continuous. Earlier continuous protonation models include a grand canonical MD algorithm developed by Mertz and Pettitt [14] in 1994 and a method introduced by Baptista et al. [15] in 1997. Later, Börjesson and Hünenberger [16, 17] developed a continuous protonation variable model using explicit solvent. The Brooks group further developed the continuous protonation state model recently [18–21]. In addition, discrete protonation state methods have also been developed for the protein pH-dependent study [22–28]. Discrete CpHMD methods combine MD and Monte Carlo (MC) sampling [29, 30], and use Metroplis criterion to accept or reject the protonation change. The Baptista group used Poisson-Boltzmann (PB) equation to calculate protonation energies [23–25]. Walczak and Antosiewicz performed Langevin dynamics between MC steps [27, 28]. Bürgi et al. calculated the transition energy by thermodynamic integration (TI) method [26].

Discrete CpHMD method was first implemented in Amber by Mongan in the year 2004 [22]. It is a model using generalized Born (GB) implicit solvation and belonging to the discrete protonation sate models. In this method, GB model [31, 32] is used in protonation state transition energy as well as solvation free energy calculations. Therefore, solvent models in conformational and sampling of protonation state are consistent, making computational cost less than other methods. This method only changes protonation states of titratable residues, which can gain or release a "ghost" proton unrealistically.

The CpHMD simulation was carried out on the Inspur TS10000 server with the parallel MD program Amber 10 [33]. The molecular docking of MOP to CquiOBP1 was performed on a Dell Precision WorkStation T5400 with the Autodock 4.0 molecular docking software package.

Preparation of systems

The X-ray crystal structure of CquiOBP1 in complex with MOP at pH 8.2 can be found in the RCSB Protein Data Bank (PDB code: 3OGN), with 1.3 Å resolution. Generally, OBPs are found as a dimer in the crystal structure, but they can slowly dissociate into corresponding monomer (active state) in solution [8]. Therefore we chose the monomeric form (chain A) of the OBPs for subsequent research. Before running the constant pH molecular dynamics, ligand MOP was deleted. Then the names of all ASP, GLU and HIS residues were changed to AS4, GL4 and HIP. This ensured that the topological parameter file *prmtop* would have a hydrogen atom defined at every possible point of protonation. After minimization, a CpHMD input file *cpin* which represented the protonation states of titrating groups should be gained for the following MD simulations.

Molecular dynamic simulations

The MD simulations were performed using the method CpHMD at pH 7 and pH 5, respectively. The ff03 force field was employed. Solvation was applied with the GB model (igb=2) [32, 34, 35]. Salt concentration (Debye-Hückel based) was set to 0.1 M, and nonbonded interactions cutoff was set to 30 Å. The time constant of Berendsen temperature bath [36] coupling for the system was 2 ps, and solute temperature used weak-coupling algorithm set to 300 K. SHAKE algorithm was chosen to constrain the lengths of bonds including hydrogen. The time step was 2 fs [22].

After minimization, the main MD simulations contained three steps, heating, equilibration and production. First, the two systems (pH 7 and pH 5) underwent 300 ps slowly heating simulations from 0 K to 300 K, respectively, with velocity of 1 K ps^{-1}. Then, we equilibrated them with another 200 ps simulation. Meantime, weak restrains were performed on the Cα atoms during the first two processes (heating and equilibration) to ensure the accomplishment of the stabilization, using the force constant as 10.0 kcal $(mol•Å^2)^{-1}$ and 1.0 kcal $(mol•Å^2)^{-1}$. After relaxation, 10 ns of MD simulations were carried out on all systems at 300 K. The final stable state of whole simulation was

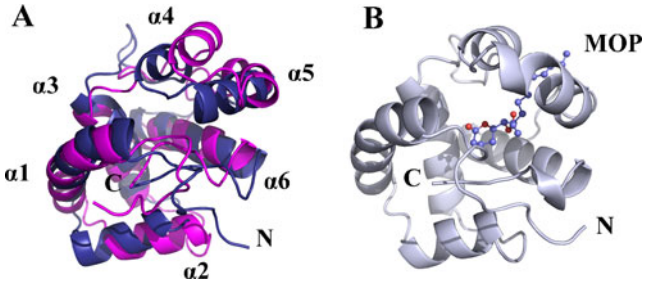

Fig. 1 Superimpositions of two three-dimensional structures **a** of CquiOBP1 in pH 7 (*deepblue*) and pH 5 (*magenta*), and the crystal structure of CquiOBP1 complex with ligand MOP (3OGN) in pH 8.2 **b**. The two structures are the lowest energy structures of the two simulations, the 3836 frame and the 3959 frame (5000 frames total), respectively. The *N* and *C* termini and six helices are labeled. Carbon atoms of ligand MOP are shown in *blue*, and oxygen atoms are colored *red*

saved as a restart point for the following molecular docking studies, and a CpHMD output file *cpout* could be obtained to reveal the predicted pKa values of each titrating residue in the systems. Additionally, two more simulations were carried out to ensure the feasibility of the CpHMD simulations. One set of the two simulations takes the last conformation of the previous pH 5 simulation and runs at pH 7; the other set uses the last conformation of the previous pH 7 simulation and performs at pH 5.

Molecular docking

Initial coordinates of CquiOBP1 for docking were obtained from the lowest energy structures during the CpHMD simulations. The structure of ligand MOP could be obtained from 3OGN [13]. Autodock 4.0, a semi-flexible docking program, was used to dock MOP into the CquiOBP1 in pH 5 and pH 7, respectively [37]. Autodock provides high quality predictions of ligand conformations with Lamarckian genetic algorithm [38]. No significant ligand-induced conformational change was detected in the structure of the CquiOBP1·MOP complex, thus ligand was treated as flexible and protein is treated as rigid [13]. Because of the existence of the original receptor in the crystal structure, prior knowledge of the binding site has been acquired. All the docking parameters used the default settings. The dimension and location settings of grid box were not changed for docking. Top ten poses ranked by binding free energy were saved for comparison and analysis. Finally, the pose with lowest value was chosen for the binding analyses.

Results and discussion

MD simulations

After 10 ns CpHMD simulations on the two systems (pH 7 and pH 5), the lowest energy structures were gained. From Fig. 1, we can easily find that there is an obvious difference in the loop regions between the two structures (pH 7 and pH 5), especially N- and C- termini loops. A hydrophobic tunnel, formed between helices α4 and α5, is relative to the ligand binding. This tunnel is in the vicinity of the binding cite in pH 7. However, the tunnel moves away from the binding site in pH 5. Consequently, we conjecture that the posture and direction of ligand binding in the CquiOBP1

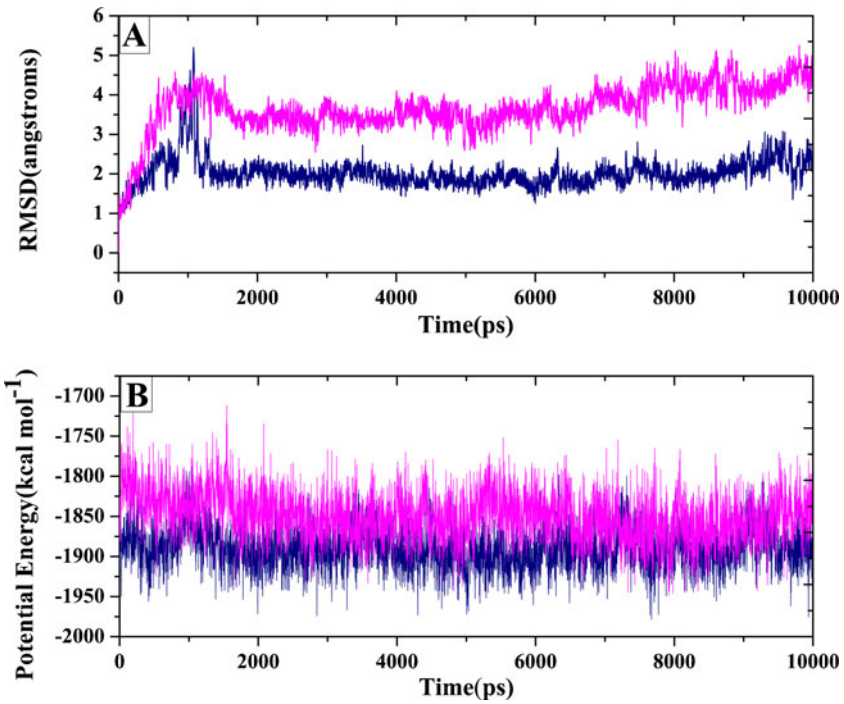

Fig. 2 **a** RMSD of CquiOBP1 alpha carbons in pH 7 (*deepblue*) and pH 5 (*magenta*) during the 10 ns molecular dynamics simulations. The RMSD value was calculated with respect to the first frame of the CpHMD simulations. **b** Potential energy profiles for the protein CquiOBP1 in pH 7 (*deepblue*) and pH 5 (*magenta*), respectively

Table 1 pKa predictions and fraction of protonation for acidic residues of CquiOBP1, calculated from 10 ns simulation starting from 3OGN at pH7 and pH5. PROPKA represents the theoretical pKa value predicted in PROPKA (http://propka.ki.ku.dk/)

	Predicted pKa			Fraction of protonation	
	pH7	pH5	PROPKA	pH7	pH5
Asp7	−∞	3.00	1.77	0.000	0.010
Asp24	3.86	2.85	3.27	0.001	0.007
Asp34	4.56	1.87	3.78	0.004	0.001
Asp42	4.28	3.84	3.18	0.002	0.065
Asp48	3.55	2.95	3.13	0.000	0.009
Asp66	2.97	3.89	2.79	0.000	0.073
Asp67	3.83	2.83	3.87	0.001	0.007
Asp70	2.81	3.16	3.77	0.000	0.014
Asp78	3.87	3.74	3.79	0.001	0.052
Asp86	3.72	3.24	3.62	0.001	0.017
Asp118	−∞	1.79	2.93	0.000	0.001
Glu9	3.80	4.95	4.65	0.001	0.469
Glu14	4.60	4.19	4.11	0.004	0.135
Glu17	4.66	4.37	4.63	0.005	0.191
Glu35	4.38	4.08	4.62	0.002	0.107
Glu39	4.94	4.75	3.12	0.009	0.363
Glu47	3.89	3.19	3.37	0.001	0.015
Glu49	3.98	3.81	3.84	0.001	0.060
Glu61	4.58	3.995	3.76	0.004	0.090
Glu74	4.235	3.858	4.50	0.002	0.067
Glu99	4.877	4.826	4.71	0.007	0.401
Glu101	4.536	4.391	4.64	0.003	0.197
Glu105	2.841	3.019	4.18	0.000	0.010
His23	7.594	5.643	6.36	0.797	0.815
His46	5.907	6.160	6.77	0.075	0.935
His60	6.305	6.296	6.47	0.168	0.952
His72	5.444	4.857	6.37	0.027	0.418
His77	6.305	5.889	6.90	0.168	0.886
His85	6.992	5.297	6.08	0.495	0.664
His90	6.667	6.154	6.01	0.317	0.934
His111	6.792	6.393	3.21	0.383	0.961
His121	6.156	7.164	6.50	0.125	0.993

would change with the transformation of the hydrophobic tunnel. Moreover, potential energy and Cα root mean square deviation (RMSD) analyses demonstrate that both the two MD simulations appear to equilibrate after 2 ns (Fig. 2). Apparently, the value of RMSD in pH 5 is stabilized near 4.0 Å, fairly higher than that in pH 7, which is straight at 2.0 Å. The results show that the structure of CquiOBP1 in pH 7 is closer to the crystal structure than that in pH 5, this proves that the protein in pH 5 undergoes a larger conformational shift, which maybe due to the influence of the ligand binding to the protein. Moreover, 2 more CpHMD simulations were performed to prove the feasibility of this method (Fig. S1). It can be found that the two simulations all have reached equilibration. After 10 ns simulation in pH 7, the last frame of the previous simulation in pH 5 takes a large conformational change, from around 5 Å to 3 Å. In the simulation from pH 7 to pH 5, the RMSD changes from 2.5 Å to 5 Å (Fig. S1a). These phenomena fit the results of the previous simulation in pH 7 and pH 5. That is to say, the protein structure will be affected by the acidic environment in pH 5 and the constant-pH MD method seems to be properly capturing the effect of pH.

It is well-known that a small change in protonation state of titrating residue can result in dramatic differences of protein conformation, and then make different binding poses of ligand [39–41]. Previously, Yang et al. [13], Lautenschlager and Xu et al. [42, 43] have proclaimed that the conformation of CquiOBP1 will be largely influenced by low pH environment. In this study, *cpout* files of Amber elucidate that CquiOBP1 has an average total molecular protonation of 19.585 at pH 7, and 26.919 at pH 5, which could result in some significant conformational changes of CquiOBP1.

There are 49 total titratable residues in CquiOBP1, including 32 acidic titratable residues and 17 basic titratable residues. Table 1 shows some relevant data of acidic titratable residues. Because of large offsets higher than 2.0 pH units, Asp34, Asp48 and Asp118 do not converge, and they are excluded for the analyses below (they have nothing to do with the important H-bonds and conformational changes). There have been no experimental pKa values of the CquiOBP1 yet, so we check the theoretical pKa values through PROPKA online (http://propka.ki.ku.dk/). Except for a few residues such as Glu39 and His111, the titrirable residues all show better agreement with theoretical pKa values. We find a crucial H-bond between amino hydrogen

Table 2 The properties of H-bonds within the pH-sensing triad in pH 7.0, includes occupied percentage, distance, angle, and lifetime

H-bond		Occupied(%)	Distance(Å)	Angle(°)	Lifetime
1	125@OXT-54@OH	44.46	2.688	19.74	10.5
2	125@O-54@OH	40.62	2.695	20.43	8.1
3	125@O-23@ND1	39.38	2.804	25.02	2.3
4	125@OXT-23@ND1	31.08	2.810	25.66	1.9
5	54@OH-23@ND1	11.46	2.883	39.10	1.3

Table 3 The properties of H-bonds within the pH-sensing triad in pH 5.0, includes occupied percentage, distance, angle, and lifetime

H-bond		Occupied(%)	Distance(Å)	Angle(°)	Lifetime
1	54@OH-23@ND1	21.90	2.864	32.54	2.1
2	125@O-23@ND1	12.62	2.778	21.33	7.4
3	23@O-54@OH	6.90	2.847	28.10	1.4

atom of Asp66 and oxygen atom of Asp 70. If this H-bond containing titratable residue is stable throughout all or nearly all of the simulation, Asp66 and Asp70 will be prevented from protonating. That H-bond will lead to very low predicted pKa values of these titratable residues. From Table 1 we can find that Asp70 shows lower predicted pKa in pH 7 than that in pH 5. H-bonds analyses treated by Amber give similar results, in pH 5, this H-bond disappears at the last part of MD simulation (distance increases to 5.5 Å in the last frame of the pH 5 simulation). This H-bond has occupied a percentage of 51.32 in pH 7, and 37.98 in pH 5 (data not shown). These two residues locate in the loop between helices α3 and α4, the disappearance of this H-bond will result in a large conformational change of this area (see Fig. 1). Besides, a similar effect can be found in Glu105 and Asn102, this H-bond leads to a very low predicted pKa in pH 7. Though with a lower percentage of occupied, this H-bond exists in the last frame of pH 5 simulation.

The cleavage of some other important H-bonds is also relevant to the conformational change between the structures in pH 7 and pH 5. The amino hydrogen atom and oxygen atom of His85 can form two H-bonds with oxygen atom of Pro81 and amino hydrogen atom of Met 89 during the pH 7 simulation, respectively. These two H-bonds are disrupted to different degrees in pH 5, which leads to the change of hydrophobic tunnel formed between helices α4 and α5. The two H-bonds between Asp7 and Tyr10 in pH 7 all disappear in pH 5, causing the considerable move of N-terminus. In addition, the oxygen atom of His60 has a hydrogen bond to amino hydrogen atom of Lys63 in pH 7, this is an important interaction between helix 3 and the loop between α3 and α4. This H-bond disappears in the last part of simulation in pH 5, contributing to the conformational change of this loop region.

H-bonds in pH-sensing triad

It is reported that the pH-sensing triad (His23-Tyr54-Val125) plays an important role in the binding and releasing of ligand [12, 13]. We have detected the relationship between the pH-sensing triad and conformational change of protein by using a series of analysis methods in Amber 10. Figure 4 illustrates that, in pH 5, the triad seems to rotate during the simulation in contrast to the conformation of CquiOBP1 in pH7. This will result in the increase of the distance though the carboxyl oxygen atom of Val125, the δ-nitrogen atom of His23, and the hydroxyl hydrogen atom of Tyr54. It is easy to find that the occupancy percentage of these H-bonds decreases and even vanishes in pH 5 (Tables 2, 3 and Fig. 3).

Concretely, there are five H-bonds through the pH-sensing triad in the pH 7 structure of CquiOBP1 (Fig. 4a), compared to the four H-bonds in pH 8.2. However, only one of them exists during the MD trajectory in pH 5, which is the H-bond 54@OH-23@ND1 (Fig. 4b). Then we calculated the distance between pH-sensing triad during the 10 ns MD simulations (carboxyl oxygen atom of Val125, the δ-nitrogen atom of His23, and the hydroxyl oxygen atom of Tyr54, Fig. 5). From Figs. 4 and 5, it is obvious that in pH 5, residue Val125 tends to depart from His23 and Tyr54, but the relative position between His23 and Tyr54 keeps steady. The H-bond (125@O-23@ND1) only stands for merely 2 ns. When the distance increases, this H-bond is disrupted. Four H-bonds between Val125 and Arg5, Val125 and Arg6 are formed in pH 5 (Fig. 6). Asp7 and Glu9 can form some

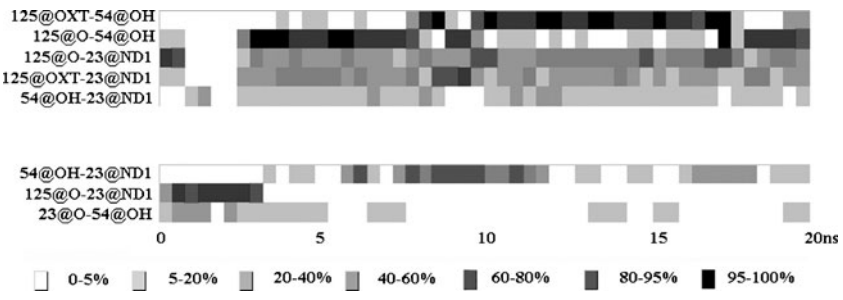

Fig. 3 The occupancy percentage of pH-sensing triad H-bonds varying with simulation time in pH 7 (*above*) and pH 5 (*below*). These H-bonds are shown in Fig. 4

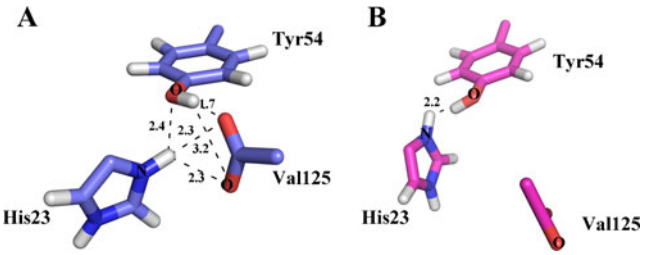

Fig. 4 Conformations comparison of the pH-sensing triad (including His23, Tyr54, and Val125) in pH 7 (**a**) and pH 5 (**b**). H-bonds are labeled with *black dashed line*. The atoms calculated for distance below are labeled with letter *O* and *N*

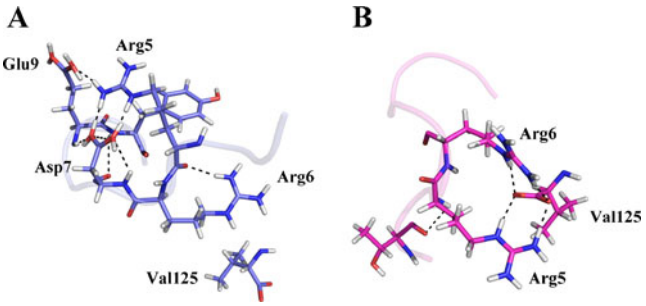

Fig. 6 The main connections between Val125 and C terminus of CquiOBP1 in pH 7 (**a**) and pH 5 (**b**), respectively. H-bonds are labeled with *black dashed lines*

important H-bonds to the Arg5 in pH 7, making N-terminus stable. With the protonation of Asp7 and Glu9, these H-bonds are disrupted in pH 5, making the carboxyl group of Val125 turn its direction to form four H-bonds to Arg5 and Arg6. This causes the movement of C-terminus in pH 5, which makes part of the binding pocket in neutral pH environment. As a result, the disruption of H-bonds in pH-sensing triad would influence the ligand binding.

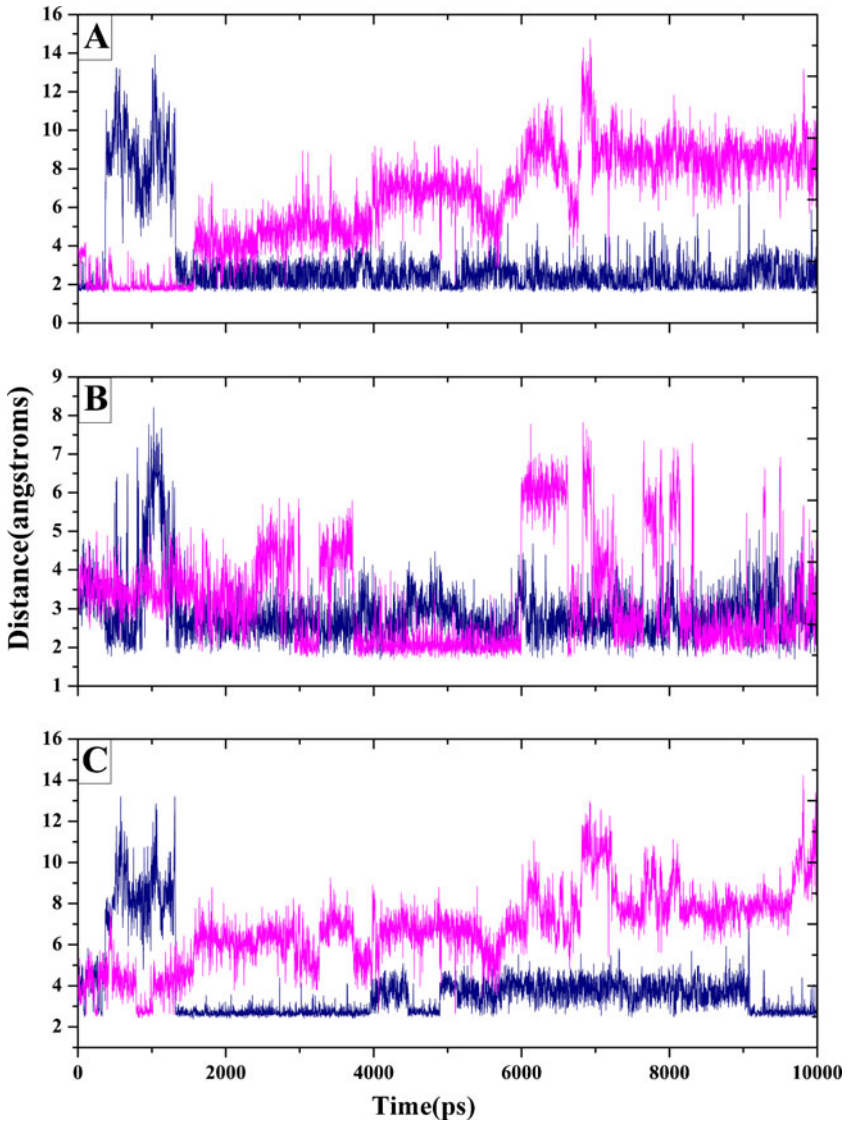

Fig. 5 Relative distance plots of pH-sensing triad, including nitrogen of His23 and oxygen of Val125 (**a**), nitrogen of His23 and hydrogen of Tyr54 (**b**), hydrogen of Tyr54 and oxygen of Val125 (**c**) in pH 7 (*deepblue*) and pH 5 (*magenta*) during 10 ns MD simulations. The three atoms for calculation are labeled in Fig. 4

Substrate binding and possible mechanics

The lowest energy structures of both dynamics trajectories in pH 7 and pH 5 were chosen for docking studies. Figure 7 gives the binding poses of MOP in pH 7 and pH 5. It shows that MOP pulls its long lipid "tail" into tunnel between helices α4 and α5 in pH 7 (Fig. 7a). The ligand holds its lactone head in the central cavity, similar to the crystal complex structure in pH 8.2. However, when it comes to the structure in pH 5, the ligand bound to the protein with a completely different pose (Fig. 7b), its head stretches out of the protein at a different direction, and its tail stays in the central cavity.

It should be noticed that the position of tunnel (α4 and α5) undergoes a movement away from the original site in pH 5, which may influence the binding posture of MOP. Also the change of loop between helices α3 and α4 and C-terminnus contributes to this. We can find that the movement of the hydrophobic tunnel tends to hinder the interaction with the tail of ligand MOP. Additionally, the distance between the lactone head of MOP and C-terminus is increasing in pH 5. These phenomena result from the protonation of some important acidic titratable residues in low pH. Base on the significant difference of ligand binding in pH 7 and pH 5, we conjecture that the ligand should be released through another tunnel between α3 and α4 in pH 5. The flexible loop between α3 and α4 is from Phe59 to Leu76, similar to the conclusion of ligand release paths in BmorPBP made by Gräter et al. [11].

Binding free energy and K_i value were calculated by Autodock 4.0 (Table 4). These data show that the system energies in pH 5 are higher than that in pH 7. Obviously, some important H-bonds are disrupted in the later part of simulation in pH 5, such as the H-bond between Asp66 and Asp70. The conformational disturbance caused by the change of pH value in solution will lead to the ligand release. For the sake of comparison, we detect the affinity of MOP to the last structure of simulation in pH 5, and notice that binding free energy is higher than −5.0 kcal mol^{-1}, K_i value increases to nearly 100 μM (not shown in Table 4). In summary, with the conformational change by protonation, some hydrophobic residues are exposed to the surface of protein, making the binding site move apart from the original position, which leads to releasing of MOP in another tunnel between α3 and α4.

Table 4 Comparison of energies and K_i value in pH 7.0 and pH 5.0

	Autodock	
	Binding free energy (kcalmol^{-1})	K_i (μM)
pH 7.0	−8.13	1.09
pH 5.0	−6.36	21.63

Conclusions

CquiOBP1 is a member of the insect odorant binding proteins family, which has conserved six α helices and three disulfide bonds, with a function to carry and transfer chemical stimulus. In solution, CquiOBP1 reveals a pH-dependent manner, which makes the protein show high affinity to its ligand at neutral pH but low affinity at low pH.

In the present study, constant pH molecular dynamics simulations (CpHMD) and molecular docking studies were performed to investigate the conformational change of CquiOBP1 in pH 7 and pH 5. The results of CpHMD show that conformation changes of CquiOBP1 in pH 5 are primarily due to the protonation of acidic titratable residues and the disruption of some important H-bonds between them. The change of protonation states will lead to the disappearance of several H-bonds in the pH-sensing triad, and the increase of relative distance between pH-sensing triad (especially the movement of Val125).

Docking studies were done for the purpose of ligand binding poses influenced by solution pH. The results indicate that MOP bound to the protein with its tail stretch into the tunnel between α4 and α5 in pH 7, similar to the condition in the crystal structure. However in pH 5, the ligand turns its direction with its head out of central cavity, and the binding free energy increases with it. Thus, another

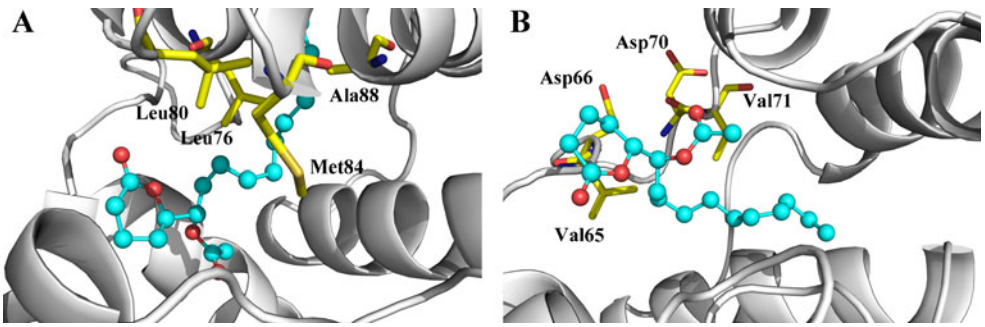

Fig. 7 Docking results using Autodock 4.0 in pH 7 (**a**) and pH 5 (**b**). Proteins are represented by the lowest energy structures in pH 7 and pH 5. Substrate MOP is shown in the *ball* and *stick* model and important residues are shown in *yellow stick*. All the oxygen atoms in MOP are colored in *red* and carbon atoms are colored in *blue*

tunnel between α3 and α4, which is formed in pH 5, will be important for the ligand MOP release. All the findings above have paved the way for the future investigation of pH-induced ligand-releasing mechanism.

Acknowledgments This work is supported by Natural Science Foundation of China, Specialized Research Fund for the Doctoral Program of Higher Education, and Specialized Fund for the Basic Research of Jilin University (Grant Nos. 20903045, 20573042, 20070183046, and 200810018).

References

1. Benton R (2006) On the origin of smell: odorant receptors in insects. Cell Mol Life Sci 63(14):1579–1585
2. Pelosi P, Calvello M, Ban L (2005) Diversity of odorant-binding proteins and chemosensory proteins in insects. Chem Senses 30 (suppl 1):i291–i292
3. Pelosi P, Zhou JJ, Ban L, Calvello M (2006) Soluble proteins in insect chemical communication. Cell Mol Life Sci 63 (14):1658–1676
4. Pelosi P, Maida R (1995) Odorant-binding proteins in insects. Comp Biochem Physiol B 111(3):503–514
5. Zhou JJ (2010) Odorant-binding proteins in insects. Vitam Horm 83:241–272
6. Chandre F, Darriet F, Darder M, Cuany A, Doannio J, Pasteur N, Guillet P (1998) Pyrethroid resistance in *Culex* quinquefasciatus from West Africa. Med Vet Entomol 12(4):359–366
7. Barbosa RMR, Furtado A, Regis L, Leal WS (2010) Evaluation of an oviposition stimulating kairomone for the yellow fever mosquito, Aedes aegypti, in Recife, Brazil. J Vector Ecol 35(1):204–207
8. Leal WS, Barbosa R, Xu W, Ishida Y, Syed Z, Latte N, Chen AM, Morgan TI, Cornel AJ, Furtado A (2008) Reverse and conventional chemical ecology approaches for the development of oviposition attractants for *Culex* mosquitoes. PLoS One 3(8):e3045
9. Horst R, Damberger F, Luginbühl P, Güntert P, Peng G, Nikonova L, Leal WS, Wüthrich K (2001) NMR structure reveals intramolecular regulation mechanism for pheromone binding and release. Proc Natl Acad Sci U S A 98(25):14374
10. Leal WS, Chen AM, Erickson ML (2005) Selective and pH-dependent binding of a moth pheromone to a pheromone-binding protein. J Chem Ecol 31(10):2493–2499
11. Gräter F, de Groot BL, Jiang H, Grubmüller H (2006) Ligand-release pathways in the pheromone-binding protein of *Bombyx mori*. Structure 14(10):1567–1576
12. Leite NR, Krogh R, Xu W, Ishida Y, Iulek J, Leal WS, Oliva G (2009) Structure of an odorant-binding protein from the mosquito *Aedes aegypti* suggests a binding pocket covered by a pH-sensitive "lid". PLoS One 4(11):e8006
13. Mao Y, Xu X, Xu W, Ishida Y, Leal WS, Ames JB, Clardy J (2010) Crystal and solution structures of an odorant-binding protein from the southern house mosquito complexed with an oviposition pheromone. Proc Natl Acad Sci U S A 107(44):19102
14. Mertz JE, Pettitt BM (1994) Molecular dynamics at a constant pH. Int J High Perform Comput Appl 8(1):47
15. Baptista AM, Martel PJ, Petersen SB (1997) Simulation of protein conformational freedom as a function of pH: constant pH molecular dynamics using implicit titration. Proteins 27(4):523–544
16. Börjesson U, Hünenberger PH (2001) Explicit-solvent molecular dynamics simulation at constant pH: methodology and application to small amines. J Chem Phys 114:9706
17. Börjesson U, Hünenberger PH (2004) pH-dependent stability of a decalysine α-helix studied by explicit-solvent molecular dynamics simulations at constant pH. J Phys Chem B 108 (35):13551–13559
18. Khandogin J, Brooks CL (2005) Constant pH molecular dynamics with proton tautomerism. Biophys J 89(1):141–157
19. Lee MS (2004) Constant-pH molecular dynamics using continuous titration coordinates. Proteins 56:738–752
20. Khandogin J, Brooks CL (2007) Linking folding with aggregation in Alzheimer's α-amyloid peptides. Proc Natl Acad Sci U S A 104 (43):16880
21. Khandogin J, Chen J, Brooks CL (2006) Exploring atomistic details of pH-dependent peptide folding. Proc Natl Acad Sci U S A 103(49):18546
22. Mongan J, Case DA, McCammon JA (2004) Constant pH molecular dynamics in generalized born implicit solvent. J Comput Chem 25(16):2038–2048
23. Baptista AM, Teixeira VH, Soares CM (2002) Constant-pH molecular dynamics using stochastic titration. J Chem Phys 117:4184
24. Machuqueiro M, Baptista AM (2006) Constant-pH molecular dynamics with ionic strength effects: protonation-conformation coupling in decalysine. J Phys Chem B 110(6):2927–2933
25. Machuqueiro M, Baptista AM (2009) Molecular dynamics at constant pH and reduction potential: application to cytochrome c 3. J Am Chem Soc 131(35):12586–12594
26. Bürgi R, Kollman PA, van Gunsteren WF (2002) Simulating proteins at constant pH: an approach combining molecular dynamics and Monte Carlo simulation. Protein Struct Funct Bioinforma 47(4):469–480
27. Dlugosz M, Antosiewicz J (2005) Effects of solute-solvent proton exchange on polypeptide chain dynamics: a constant-pH molecular dynamics study. J Phys Chem B 109 (28):13777–13784
28. Walczak AM, Antosiewicz JM (2002) Langevin dynamics of proteins at constant pH. Phys Rev E 66(5):051911
29. Williams SL, De Oliveira CAF, McCammon JA (2010) Coupling constant pH molecular dynamics with accelerated molecular dynamics. J Chem Theory Comput 6(2):560–568
30. Meng Y, Roitberg AE (2010) Constant pH replica exchange molecular dynamics in biomolecules using a discrete protonation model. J Chem Theory Comput 6(4):1401–1412
31. Bashford D, Case DA (2000) Generalized born models of macromolecular solvation effects. Annu Rev Phys Chem 51 (1):129–152
32. Onufriev A, Bashford D, David A (2000) Modification of the generalized born model suitable for macromolecules. J Phys Chem B 104(15):3712–3720
33. Case DA, Darden T, Cheatham III TE, Simmerling C, Wang J, Duke RE, Luo R, Crowley M, Walker R, Zhang W (2008) Amber 10 users manual. University of California
34. Onufriev A, Case DA, Bashford D (2002) Effective Born radii in the generalized born approximation: the importance of being perfect. J Comput Chem 23(14):1297–1304
35. Onufriev A, Bashford D, Case DA (2004) Exploring protein native states and large-scale conformational changes with a modified generalized born model. Proteins 55(2):383–394
36. Berendsen HJC, Postma JPM, Van Gunsteren WF, DiNola A, Haak J (1984) Molecular dynamics with coupling to an external bath. J Chem Phys 81:3684
37. Morris GM, Huey R, Lindstrom W, Sanner MF, Belew RK, Goodsell DS, Olson AJ (2009) AutoDock4 and AutoDockTools4: automated docking with selective receptor flexibility. J Comput Chem 30(16):2785–2791
38. Morris GM, Goodsell DS, Halliday RS, Huey R, Hart WE, Belew RK, Olson AJ (1998) Automated docking using a Lamarckian

genetic algorithm and an empirical binding free energy function. J Comput Chem 19(14):1639–1662
39. Sham YY, Muegge I, Warshel A (1998) The effect of protein relaxation on charge-charge interactions and dielectric constants of proteins. Biophys J 74(4):1744–1753
40. Simonson T, Archontis G, Karplus M (1999) A Poisson-Boltzmann study of charge insertion in an enzyme active site: the effect of dielectric relaxation. J Phys Chem B 103(29):6142–6156
41. Warshel A, Aqvist J (1991) Electrostatic energy and macromolecular function. Annu Rev Biophys Biophys Chem 20(1):267–298
42. Lautenschlager C, Leal WS, Clardy J (2005) Coil-to-helix transition and ligand release of *Bombyx mori* pheromone-binding protein. Biochem Biophys Res Commun 335(4):1044–1050
43. Xu W, Leal WS (2008) Molecular switches for pheromone release from a moth pheromone-binding protein. Biochem Biophys Res Commun 372(4):559–564